

Gibbs Sampling using Anti-correlation Gaussian Data Augmentation, with Applications to L1-ball-type Models

Yu Zheng ^{*} Leo L. Duan [†]

Abstract

L1-ball-type priors are a recent generalization of the spike-and-slab priors. By transforming a continuous precursor distribution to the L1-ball boundary, it induces exact zeros with positive prior and posterior probabilities. With great flexibility in choosing the precursor and threshold distributions, we can easily specify models under structured sparsity, such as those with dependent probability for zeros and smoothness among the non-zeros. Motivated to significantly accelerate the posterior computation, we propose a new data augmentation that leads to a fast block Gibbs sampling algorithm. The latent variable, named “anti-correlation Gaussian”, cancels out the quadratic exponent term in the latent Gaussian distribution, making the parameters of interest conditionally independent so that they can be updated in a block. Compared to existing algorithms such as the No-U-Turn sampler, the new blocked Gibbs sampler has a very low computing cost per iteration and shows rapid mixing of Markov chains. We establish the geometric ergodicity guarantee of the algorithm in linear models. Further, we show useful extensions of our algorithm for posterior estimation of general latent Gaussian models, such as those involving multivariate truncated Gaussian or latent Gaussian process.

Keywords: Blocked Gibbs sampler; Fast Mixing of Markov Chains; Latent Gaussian Models; Soft-thresholding.

^{*}Department of Statistics, University of Florida, zheng.yu@ufl.edu

[†]Department of Statistics, University of Florida, li.duan@ufl.edu

1 Introduction

There is a large literature on Bayesian sparse models and the inspired algorithms for estimating the posterior. Originally motivated for solving the variable selection problem in linear regression, spike-and-slab priors (or, “discrete spike-and-slab”, [Tadesse and Vannucci 2021](#)) have the marginal form of a two-component mixture for each parameter element: one component (spike) from a point mass at zero, and the other (slab) from a continuous distribution ([Mitchell and Beauchamp, 1988](#)); the continuous elements can be independent or dependent a priori. For linear regression with Gaussian errors, very efficient Markov chain Monte Carlo (MCMC) algorithms have been developed. When the slab prior distribution follows a Gaussian, the Stochastic Search Variable Selection (SSVS) algorithm ([George and McCulloch, 1995](#)) exploits the posterior conjugacy and samples from the marginal posterior of the binary inclusion variables. SSVS is a Gibbs sampler that tries to flip each binary inclusion variable one at a time from a Bernoulli full conditional distribution; at the end of each iteration, it samples the regression coefficients given the vector of binary inclusion variables. As an alternative to using the marginal posterior, the Orthogonal Data Augmentation (ODA) algorithm ([Ghosh and Clyde, 2011](#)) introduces an augmented design matrix (along with augmented responses) to append the observed design matrix, such that the Gram matrix becomes diagonal hence easily invertible, enabling the use of two-block Gibbs sampler. The ODA algorithm can be extended to some generalized linear models if the latent Gaussian has a fixed variance, such as probit regression ([Albert and Chib, 1993](#)). Further, for design matrix that is high-dimensional or contains highly correlated predictors, various algorithms have been proposed such as shotgun algorithm ([Hans et al., 2007](#)), parallel tempering ([Bottolo and Richardson, 2010](#)), correlation-based search ([Kwon et al., 2011](#)), two-parameter flipping Metropolis-Hastings algorithm under g -prior slab ([Yang et al., 2016](#)). In the meantime, there is a comparably vast literature on continuous shrinkage priors with excellent performance for the task of variable selection ([George and McCulloch, 1995](#); [Rocková and George, 2018](#); [Polson and Scott, 2010](#); [Carvalho et al., 2010](#); [Piironen and Vehtari, 2017](#); [Armagan et al., 2013](#); [Bhattacharya et al., 2015](#); [Bai and Ghosh, 2019](#)). Since our focus is on the posterior with exact zeros, for brevity, we will skip the detail of continuous shrinkage.

With the rich literature, there is a recent interest in structured sparsity ([Hoff, 2017](#); [Griffin and Hoff, 2023](#)) that has inspired new extensions of sparsity priors. Specifically, the sparsity is “structured” in the sense that: (i) the occurrences of zeros could be dependent, according to some temporal, spatial, or group structure;

(ii) the non-zeros could have some correlation structure, such as smoothness over some spatial domain. We now provide a few examples. In the task of change-point detection, one may model a time series as having the mean increments to be sparse over a continuous period of time so that the mean function would become a step function (Tibshirani et al., 2005; Betancourt et al., 2017). In the scalar-on-image regression, one may model the regression coefficients to be spatially smooth for those non-zeros, while being zero over several continuous regions (Kang et al., 2018). For these models, a critical computational challenge arises that the above existing algorithms for spike-and-slab priors cannot be applied directly here, due to the lack of conjugacy or fixed variance for latent Gaussian. Because of the correlations among the elements of the parameter, updating the full conditional of one element at a time suffers from slow mixing of Markov chains. To facilitate the model development and posterior estimation under structured sparsity, (Xu and Duan, 2023) propose the L1-ball priors: starting with a continuous random variable $\beta \in \mathbb{R}^p$ from a “precursor” distribution (that could be correlated or smooth over some input space), one projects β to the boundary of the L1 ball. This projection produces θ containing exact zeros with positive probability (in both prior and posterior). To explain the gist of the idea, we focus on the equivalent generative process using soft-thresholding transform:

$$\beta \sim \pi_0^\beta, \quad \theta = \text{sign}(\beta) \circ (|\beta| - \kappa)_+, \quad (1.1)$$

where the operation is conducted element-wise in the second term, and $(\cdot)_+$ is the truncation function to $[0, \infty)$. In the projection to L1-ball with L1-norm $\theta \in \mathbb{R}^p : \|\theta\|_1 \leq r$ for some $r > 0$, $\kappa > 0$ is a scalar output from a deterministic transformation of (β, r) , as shown in (Xu and Duan, 2023). On the other hand, one could generalize κ to be another free non-negative parameter or a vector of non-negative values. Therefore, we refer to the generalized class of (1.1) as the L1-ball-type priors or models. As one motivating example (that we will revisit later), the soft-thresholded Gaussian process prior (Kang et al., 2018) is built with β from a Gaussian process and κ as a scalar. This prior enjoys a nice property that θ is continuous over the input domain with high sparsity at the same time, hence is particularly useful for selecting sub-regions of an image for regression or smoothing.

Focusing on the computational aspect, the soft-thresholding transform is differentiable almost everywhere with respect to π_0^β . This means we can use off-the-shelf gradient-based MCMC algorithms (Duane et al., 1987; Girolami and Calderhead, 2011; Hoffman and Gelman, 2014; Livingstone and Zanella, 2022)

for its posterior estimation. The strength of these algorithms, besides low implementation cost due to the good accessibility of software (Carpenter et al., 2017; Bingham et al., 2019), is in the rapid convergence to the region near the posterior mode and a high acceptance rate for changing the zero/non-zero status of multiple elements at the same time. On the other hand, notice that if the likelihood is parameterized via θ and κ but not dependent on β a priori, then at the state with some $\theta_j = 0$, the partial derivative of the log-posterior density with respect to β_j is zero. As a consequence, the algorithm relying on one-step diffusion [such as Metropolis-adjusted Langevin algorithm (MALA) (Rossky et al., 1978)] would be not efficient to explore changing θ_j to a non-zero state. That is why multiple-step diffusion algorithms such as Hamiltonian Monte Carlo (Neal, 2011) and No-U-Turn sampler (Hoffman and Gelman, 2014) are preferable.

Since multiple evaluations of the gradient can be expensive, there is room for improvement that can be made in terms of gaining computational efficiency. This motivates us to do exploration in the class of Gibbs samplers, which tends to have a very low computing cost per iteration and requires almost no tuning. To avoid one-element-at-a-time Gibbs sampling, we introduce an augmented latent variable that allows us to cancel out the interaction term among the parameter elements. This enables us to update the elements in a block in each iteration. We show that this new algorithm achieves much higher efficiency in terms of effective sample size per time unit. Further, we establish the geometric ergodicity guarantee in linear regression. Interestingly, our proposed latent variable is broadly applicable beyond the L1-ball-type model setting and can be applicable in the challenging cases of estimating latent Gaussian models, such as those involving multivariate truncated Gaussian or latent Gaussian process. The source code is available on <https://github.com/YuZh98/Anti-correlation-Gaussian>.

2 Blocked Gibbs Sampling with Anti-correlation Latent Gaussian

2.1 Motivating Problems

We now introduce the motivating sampling problem and provide the necessary notations. Let $\theta \in \mathbb{R}^p$ be the parameter of interest, associated with precursor random variable $\beta \in \mathbb{R}^p$ via (1.1). We use \mathcal{Y} to denote the data, where $\mathcal{Y}_i = (x_i, y_i)$ with y_i as outcome and x_i as predictor. With some loss of generality, we

focus on the following form on the conditional posterior:

$$\begin{aligned} \Pi(\theta, \beta \mid M, \phi, H, \psi, \kappa, \mathcal{Y}) &\propto \exp \left[-\frac{1}{2}(\theta' M \theta - 2\phi' \theta) \right] \exp \left[-\frac{1}{2}(\beta' H \beta - 2\psi' \beta) \right], \\ \theta &= \text{sign}(\beta) \circ (|\beta| - \kappa)_+, \end{aligned} \quad (2.1)$$

where M and H are both positive semi-definite matrix of size $p \times p$, $\phi \in \mathbb{R}^p$, $\psi \in \mathbb{R}^p$, and $\kappa \in \mathbb{R}^p$. We treat κ as given for now, but will discuss the case when κ is assigned with another prior.

Although the first line in (2.1) resembles a product of two latent Gaussian densities, the equality constraint in the second line makes it a degenerate density. A formal notation for the degenerate density can be obtained using infinitesimal

$$p(d\theta, d\beta \mid H, \kappa, \psi) = p(\beta \mid H, \psi) \delta_{T_\kappa(\beta)}(d\theta) d\beta, \quad T_\kappa(\beta) = \text{sign}(\beta) \circ (|\beta| - \kappa)_+,$$

where δ is the Dirac measure. On the other hand, for the ease of notation, we will stick to the simplified form (2.1) in this article. We now provide three concrete examples to illustrate the generality of the above types of problems.

In a linear regression model for $y = X\theta + \epsilon$, with a predictor matrix $X \in \mathbb{R}^{n \times p}$, $\epsilon \sim \text{N}(0, \Omega^{-1})$ for some positive definite Ω , and independent Gaussian precursor $\beta_j \stackrel{\text{indep}}{\sim} \text{N}(0, \tau_j)$ for some given hyper-parameter $\tau_j > 0$. We have (2.1) with $M = X' \Omega X$, $\phi = X' \Omega y$, $H = \text{diag}(1/\tau_j)$ and $\psi = 0$.

In a logistic regression model with binary $y_i \sim \text{Bernoulli}[1/(1 + \exp(-x_i' \theta))]$, we can use the Polya-Gamma data augmentation to create a Gaussian augmented likelihood (see [Polson et al. 2013](#) for detail). Under independent Gaussian precursor $\beta_j \stackrel{\text{indep}}{\sim} \text{N}(0, \tau_j)$, we have (2.1) with $M = X' \Omega X$, $\phi = X' \Omega (y - 1/2)$, $H = \text{diag}(1/\tau_j)$, $\psi = 0$, and $\Omega = \text{diag}(\omega_j)$ with ω_j marginally from the Polya-Gamma distribution $\text{PG}(1, 0)$.

In a sparse smoothing model $y = \theta + \epsilon$, with $\epsilon \sim \text{N}(0, I\sigma^2)$, y_i associated with some spatial coordinate s_i , for which the goal is to obtain a spatially correlated θ_i , while making some θ_i 's zero in some contiguous regions of s_i 's. We can use a spatially correlated Gaussian precursor $\beta \sim \text{N}[0, K(s, s)]$ with K some covariance kernel such as the squared exponential kernel. We have (2.1) with $M = I\sigma^{-2}$, $\phi = y\sigma^{-2}$, $H = [K(s, s)]^{-1}$ and $\psi = 0$.

For any non-diagonal M or H , the quadratic term $\theta' M \theta$ or $\beta' H \beta$ in the exponent of (2.1) makes it difficult to explore a large change in the parameter. This motivates us to use some latent variables to cancel out those terms.

2.2 Anti-correlation Gaussian

If M is non-diagonal and we want to cancel out $\theta' M \theta$, consider a Gaussian latent variable $r \in \mathbb{R}^p$:

$$(r \mid \theta, M) \sim \mathcal{N}[(dI - M)\theta, (dI - M)], \quad (2.2)$$

where $d > \lambda_p(M)$ is a chosen constant to make $dI - M$ positive definite, with $\lambda_p(\cdot)$ the spectral norm. Similarly, if H is non-diagonal, we use

$$(t \mid \beta, H) \sim \mathcal{N}[(eI - H)\beta, (eI - H)], \quad (2.3)$$

with $e > \lambda_p(H)$.

We refer to (2.2) as an “anti-correlation Gaussian”, because it cancels out the quadratic correlation terms. For brevity, from now on, we focus on the case when we use both r and t , and we can see that the conditional posterior of (β_j, θ_j) becomes independent over j :

$$\begin{aligned} \Pi(\beta, \theta \mid M, \phi, H, r, t, \kappa, \mathcal{Y}) &\propto \prod_{j=1}^p \exp \left\{ -\frac{1}{2} [d\theta_j^2 - 2(\phi_j + r_j)\theta_j + e\beta_j^2 - 2(\psi_j + t_j)\beta_j] \right\}, \\ \theta_j &= \text{sign}(\beta_j)(|\beta_j| - \kappa_j)_+. \end{aligned} \quad (2.4)$$

The conditional independence allows us to draw β_j ’s in a block. It is not hard to see that each β_j follows a three-component mixture, corresponding to the cases when $\theta_j > 0$, $\theta_j = 0$ or $\theta_j < 0$, for which we take a discrete variable b_j taking value 1, 0 or -1 , respectively. We have b_j in the following:

$$\begin{aligned} \Pi(b_j = 0 \mid \cdot) &= c_j^{-1} m_0^{-1} \exp \left[\frac{1}{2} \frac{(\psi_j + t_j)^2}{e} \right], \\ \Pi(b_j = 1 \mid \cdot) &= c_j^{-1} m_1^{-1} \exp \left[\frac{1}{2} \frac{(\phi_j + r_j + \psi_j + t_j + d\kappa_j)^2}{d + e} - \frac{1}{2} d\kappa_j^2 - (\phi_j + r_j)\kappa_j \right] \\ \Pi(b_j = -1 \mid \cdot) &= c_j^{-1} m_{-1}^{-1} \exp \left[\frac{1}{2} \frac{(\phi_j + r_j + \psi_j + t_j - d\kappa_j)^2}{d + e} - \frac{1}{2} d\kappa_j^2 + (\phi_j + r_j)\kappa_j \right], \end{aligned} \quad (2.5)$$

where we use $\Pi(b \mid \cdot)$ as a shorthand notation for the full conditional posterior of b . In the above, c_j^{-1} is a normalizing constant to make the three probabilities add up to one; m_0 , m_1 and m_{-1} are the constants in the following truncated Gaussian

densities (2.6) that multiplied to the exponential terms:

$$\begin{aligned}
(\beta_j \mid b_j = 0, \cdot) &\sim N_{(-\kappa_j, \kappa_j)}\left(\frac{\psi_j + t_j}{e}, \frac{1}{e}\right), \\
(\beta_j \mid b_j = 1, \cdot) &\sim N_{(\kappa_j, \infty)}\left(\frac{\phi_j + r_j + \psi_j + t_j + d\kappa_j}{d + e}, \frac{1}{d + e}\right), \\
(\beta_j \mid b_j = -1, \cdot) &\sim N_{(-\infty, -\kappa_j)}\left(\frac{\phi_j + r_j + \psi_j + t_j - d\kappa_j}{d + e}, \frac{1}{d + e}\right),
\end{aligned} \tag{2.6}$$

where the subscript in $N_{(\tilde{\alpha}_1, \tilde{\alpha}_2)}$ denotes the support of the truncated Gaussian. Therefore, we can draw each b_j first, and then β_j from the corresponding truncated Gaussian. Note that θ is completely determined once β and κ are given. As a result, besides the other parameters, we have a two-block update scheme based on sampling $(r, t \mid \beta, \cdot)$, and sampling $(\beta \mid r, t, \cdot)$. See Algorithm 1 below.

Remark 2.1. *In the above, we present the simple case when each κ_j is given. How to estimate κ_j in MCMC depends on the structure and prior one imposes on the vector κ . In the examples of this article, we use a common $\kappa_j = \kappa_0$ for all j , and prior $\pi_0(\kappa_0)$. We use slice sampling step to update κ_0 , with $\Pi(\kappa_0 \mid \cdot) \propto \pi_0(\kappa_0)\Pi(\theta, \beta \mid M, \phi, H, \psi, \kappa_0, \mathcal{Y})$ where the second term is from (2.4). We sample the other parameters (such as the variance of measurement error) from their respective full conditional distribution.*

Empirically, we find the values of $d > \lambda_p(M)$ and $e > \lambda_p(H)$ have almost no effects on the mixing performance (Appendix B.6), as long as the values do not lead to numerical overflow. In this article, since our cost of computing upper bounds $\tilde{\lambda}_p(M) \geq \lambda_p(M)$ or $\tilde{\lambda}_p(H) \geq \lambda_p(H)$ is negligibly low in each iteration of MCMC (as described in the next section), we set $d = \tilde{\lambda}_p(M) + \varepsilon$, $e = \tilde{\lambda}_p(H) + \varepsilon$, and ε is set to 10^{-6} . For general M and H , one can use Frobenius norm as an upper bound for $\lambda_p(M)$ or $\lambda_p(H)$.

2.3 Efficient Sampling of the Anti-Correlation Gaussian in Regression

We now focus on making the sampling of the anti-correlation Gaussian more efficient for large p . Motivated by regression settings and with some loss of generality, we focus on the scenario where M is updated as a three-matrix product $M = X'\Omega X$, where X is fixed but Ω can change in each iteration. For simplicity, we focus on sampling of $r \sim N[(dI - M)\theta, (dI - M)]$, and the method is trivially extensible to the sampling of t , if needed.

Algorithm 1: Anti-correlation Blocked Gibbs Sampler

```

for  $k \leftarrow 1$  to  $K$  do
    Sample  $(r^k, t^k)$  from (2.2) and (2.3);
    Sample  $\beta^k$  from (2.5) and (2.6);
    Sample  $\kappa^k$  from the full conditional distribution;
    Compute  $\theta^k$  via the second line of (2.4);
    Sample the other parameters (if needed) from the respective full
    conditional distribution.

```

Canonically, sampling this multivariate Gaussian involves decomposing the covariance matrix $(dI - X'\Omega X)$, which is an $\mathcal{O}(p^3)$ operation. In the case of simple regression with homoscedasticity $\Omega = I\sigma^{-2}$ (such as linear regression with homoscedasticity, or the latent Gaussian in probit regression with $\sigma^2 = 1$, [Albert and Chib 1993](#)), we could use $d = (\lambda_p(X'X) + \tilde{\epsilon})\sigma^{-2}$ with a small $\tilde{\epsilon} > 0$, then we only need to decompose $(d\sigma^2 I - X'X) = \mathcal{L}\mathcal{L}'$ for one time before the start of the Markov chain. In each Markov chain iteration, we can sample r efficiently via $r = \sigma^{-1}\mathcal{L}\gamma_1 + (dI - M)\theta$ with $\gamma_1 \sim \mathcal{N}(0, I_p)$.

On the other hand, when Ω is more complicated than $I\sigma^{-2}$, and is updated in every iteration (such as in logistic regression where Ω is updated from a Polya-Gamma distribution), we would need to compute the decomposition each time. Similar issues have been noted by [Bhattacharya et al. \(2016\)](#) and [Nishimura and Suchard \(2022\)](#) during the sampling of a Gaussian with covariance $(X'\Omega X + D)^{-1}$ with D positive definite, the first group of authors exploits the Woodbury matrix identity and involves an inversion of an $n \times n$ matrix, and the second group uses a preconditioned conjugate gradient method to iteratively solve a linear system. Here our problem is slightly different, in the form of sampling of a Gaussian with covariance $(dI - X'\Omega X)$ (or equivalently, a transform $r = (dI - X'\Omega X)\gamma_2$, with $\gamma_2 \sim \mathcal{N}[\theta, (dI - X'\Omega X)^{-1}]$). The subtraction in the covariance/precision matrix creates a new challenge, for which we develop a new non-iterative algorithm.

For ease of presentation, we now focus on the $p \geq n$ case, and one can modify it to accommodate the $p \leq n$ case easily. Before the start of the Markov chain, we pre-compute the singular value decomposition (SVD) of $X = U_X \Lambda_X V_X'$, with U_X an $n \times n$ matrix, V_X an $p \times n$ matrix, Λ_X an $n \times n$ diagonal matrix with diagonal entries $\Lambda_{X,(i,i)} \geq 0$ for $i = 1, \dots, n$. We denote $\Lambda_X^* := \Lambda_{X,(1,1)}$ as the largest singular value, and $b_\Omega := [\lambda_n(\Omega)]^{-1}$ with $\lambda_n(\Omega)$ the largest eigenvalue of Ω . We assume $d > \lambda_n(\Omega)(\Lambda_X^*)^2$, which is sufficient to ensure positive definiteness of

$dI - X'\Omega X$. Further, we obtain a matrix $V_X^\dagger \in \mathbb{R}^{p \times (p-n)}$ such that $[V_X \ V_X^\dagger]$ forms an orthonormal matrix, using the full SVD of X .

Remark 2.2. *The SVD is computationally expensive for large n or p . Fortunately, we only need to run SVD for one time before starting MCMC. The following sampler for r does not involve any matrix decomposition or inversion when running MCMC. With vectorized computation on matrix-vector products, each MCMC iteration has a parallel run time $\mathcal{O}[\max(n, p)]$.*

We use the following sampling scheme.

1. Sample $\gamma_1 \sim N(0, dI_n)$, $\gamma_2 \sim N(0, dI_{p-n})$, $\gamma_3 \sim N[\Lambda_X \gamma_1 / d, b_\Omega I_n - (\Lambda_X)^2 / d]$;
2. Sample $\eta \sim N(0, \Omega^{-1} - b_\Omega I_n)$;
3. Set $r = V_X \gamma_1 + V_X^\dagger \gamma_2 - X' \Omega (U_X \gamma_3 + \eta) + (dI - X' \Omega X) \theta$.

In the above, the Gaussian could be degenerate with zero variance for some elements.

Theorem 2.1. *The above algorithm produces a random sample from the anti-correlation Gaussian, $r \sim N[(dI - X' \Omega X) \theta, (dI - X' \Omega X)]$.*

Proof. It is not hard to see that

$$\begin{bmatrix} \gamma_1 \\ \gamma_2 \\ \gamma_3 \end{bmatrix} \sim N\left(\begin{bmatrix} 0 \\ 0 \\ 0 \end{bmatrix}, \begin{bmatrix} dI_n & O & \Lambda_X \\ O & dI_{p-n} & O \\ \Lambda_X & O & b_\Omega I_n \end{bmatrix}\right), \text{ and } \begin{bmatrix} V_X \gamma_1 + V_X^\dagger \gamma_2 \\ U_X \gamma_3 + \eta \end{bmatrix} \sim N\left(\begin{bmatrix} 0 \\ 0 \end{bmatrix}, \begin{bmatrix} dI_p & X' \\ X & \Omega^{-1} \end{bmatrix}\right),$$

where O in the above denotes a conformable matrix filled with zeros. The first covariance is positive definite because $db_\Omega > \Lambda_{X,i,i}^2$ for any $i = 1, \dots, n$. Then we see that $\text{VAR}[V_X \gamma_1 + V_X^\dagger \gamma_2 - X' \Omega (U_X \gamma_3 + \eta)] = dI + X' \Omega \Omega^{-1} \Omega X - 2X' \Omega X = dI - X' \Omega X$. Adding $(dI - X' \Omega X) \theta$ yields the result. \square

We now discuss the complexity of the above sampling algorithm. The sampling of γ_1 , γ_2 , and γ_3 can be carried out very efficiently due to the diagonal covariance. Often Ω is a diagonal matrix, hence sampling of η can be quite efficient as well. For the other cases with non-diagonal Ω at a large n , one often adopts a structured (such as close-to-low-rank) Ω or Ω^{-1} under which η can be sampled efficiently (Ghosh and Dunson, 2009; Chandra et al., 2021).

3 Geometric Ergodicity Guarantee

Now we establish the convergence guarantee of our proposed Gibbs sampling algorithm for linear models. For mathematical tractability, we focus on the models with fixed $(M, \phi, H, \psi, \kappa)$, hence the two-block updating scheme. Since κ is assumed fixed, θ is uniquely determined by β . In order to avoid the complication from degenerate distribution, we only focus on β and (r, t) in the context of the distribution or measure.

Our target distribution is associated with the joint posterior probability kernel function for (β, r, t) :

$$\Pi(r, t \mid M, H, \beta) \Pi(\beta \mid M, \phi, H, \psi, \kappa, \mathcal{Y}),$$

and we denote the associated measure by $\mu_{\beta, r, t}(\cdot)$. In MCMC, we start with initial values for those latent variables drawn from a certain initial distribution, and we denote them by (r^0, t^0) , then we update their values iterative via the following Markov transition kernel:

$$\begin{aligned} & \mathcal{K}(\beta^{m+1}, r^{m+1}, t^{m+1} \mid r^m, t^m) \\ &= \Pi_{\mathcal{K}}(r^{m+1}, t^{m+1} \mid \beta^{m+1}) \Pi_{\mathcal{K}}(\beta^{m+1} \mid r^m, t^m) \end{aligned}$$

for $m = 0, 1, 2, \dots$, where the first two densities are based on (2.2) and that of t , and the last one is based on (2.5) and (2.6), with all the fixed parameters omitted. We denote the associated measure for (β^m, r^m, t^m) by $P_{\beta, r, t}^m[(r^0, t^0), \cdot]$.

In order to show that $P_{\beta, r, t}^m[(\beta^0, r^0, t^0), \cdot]$ converges to $\mu_{\beta, r, t}(\cdot)$, we can simply show that $P_{r, t}^m[(r^0, t^0), \cdot]$ converges to $\mu_{r, t}(\cdot)$, with $\mu_{r, t}(\cdot)$ the marginal posterior measure integrated over β , and $P_{r, t}^m[(r^0, t^0), \cdot]$ the marginal measure of (r^m, t^m) after m MCMC iterations after integrating out β^m . A similar technique was used by Tan et al. (2013) for a two-part update scheme. With those ingredients in place, we are ready to state the geometric ergodicity results.

Theorem 3.1. *There exists a real-valued function $C_1(r^0, t^0)$ and $0 < \gamma < 1$ such that for all (r, t) ,*

$$\|P_{r, t}^m[(r^0, t^0), \cdot] - \mu_{r, t}(\cdot)\|_{TV} \leq C_1(r^0, t^0) \gamma^m, \quad (3.1)$$

where $\|\cdot\|_{TV}$ denotes the total variation norm.

We defer the proof to Appendix A. Further, we have the following result.

Theorem 3.2. *The Markov chain generated by $\mathcal{K}(\beta^{m+1}, r^{m+1}, t^{m+1} \mid \beta^m, r^m, t^m)$ is geometrically ergodic. Specifically, there exists a real-valued function $C_2(r^0, t^0)$ and $0 < \gamma < 1$ such that for all (r^0, t^0) ,*

$$\|P_{(\beta, r, t)}^m[(r^0, t^0), \cdot] - \mu_{(\beta, r, t)}(\cdot)\|_{TV} \leq C_2(r^0, t^0)\gamma^m, \quad (3.2)$$

where γ is the same rate as the one in (3.1).

The proof is a direct extension of Theorem 3.1, since $\Pi_{\mathcal{K}}(\beta \mid r, t)$ in the Markov transition kernel after m iterations and $\Pi(\beta \mid r, t, M, \phi, H, \psi, \kappa, \mathcal{Y})$ in the posterior distribution are the same thing. Therefore, the convergence rate remains the same. See Diaconis et al. (2008); Liu et al. (1994); Robert (1995); Roberts and Rosenthal (2001) for detail.

Remark 3.1. *To be rigorous, we obtain the above convergence theory for the two-block data augmentation sampler. For more complicated samplers that involve more than two blocks (such as those in our numerical examples), we observe fast empirical convergence and hence expect the theory to be generalizable.*

Remark 3.2. *Our convergence result is only qualitative, and getting a rate quantification of γ is challenging and beyond the scope of this article. We refer the readers to Qin et al. (2019) for useful analytical techniques that could lead to a tractable rate calculation. In Appendix B.2, we provide numerical evidence of fast convergence for dimensions up to $p = 5000$.*

On computational efficiency, a data augmentation-based Gibbs sampler, which alternates in drawing from $\Pi(\theta \mid r, y, \cdot)$ and $\Pi(r \mid \theta, y, \cdot)$ in closed forms, often has a slower mixing rate than a marginal sampler targeting $\Pi(\theta \mid y, \cdot) = \int \Pi(\theta, r \mid y, \cdot)dr$. However, when there lacks a closed form for drawing from the marginal $\Pi(\theta \mid y, \cdot)$, one has to rely on computationally expensive Markov transition kernel (such as No-U-Turn leapfrog steps) to update θ . Therefore, there is a balance to be struck — in order to produce a fixed size m effective samples of θ 's, one either runs (i) a marginal density-based algorithm that is relatively slow in each iteration but with fast mixing (hence fewer iterations needed), or (ii) a data augmentation-based algorithm that is fast in each iteration but with relatively slow mixing (hence more iterations needed). Clearly, one would prefer the algorithm that takes a shorter time to produce m effective samples, as measured by a higher effective sample size per time unit (ESS/time). We provide empirical evidence in Section 5.1 that our data augmentation-based sampler has a higher ESS/time than some popular marginal density-based sampler.

4 Extensions

The data augmentation using anti-correlation Gaussian can be employed beyond the scope of L1-ball-type models. We now discuss two useful classes of extensions.

The first extension is on the sampling of latent Gaussian models (Robert and Casella, 2004; Fahrmeir and Tutz, 2001; Gelman, 2014), whose likelihood generally takes the form:

$$L(y; \theta) \propto \int |M(\theta)|^{1/2} \exp \left[-\frac{1}{2} z^T M(\theta) z \right] \prod_{i=1}^n g(y_i | z_i, \theta) dz, \quad (4.1)$$

with g some density/mass function for the data y , and $M(\theta)$ is a positive definite matrix that depends on θ as the parameter of interest. This framework covers a wide range of applications such as spatial, regression, or dynamic modeling. Although it seems intuitive to simply sample z as a latent variable during MCMC, the presence of non-Gaussian g often disrupts posterior conjugacy, creating difficulty in efficiently updating z especially when z is in high dimension. This is one major motivation for posterior approximation methods such as integrated nested Laplace approximation (INLA) (Rue et al., 2009) as an alternative to MCMC.

Using the anti-correlation Gaussian ($r | z, \theta \sim N\{[dI - M(\theta)]z, dI - M(\theta)\}$), we can obtain conditionally independent z_i that can be updated efficiently in a block.

$$\Pi(z | r, \theta, y) \propto \prod_{i=1}^n g(y_i | z_i, \theta) \exp\left(-\frac{1}{2} dz_i^2 + z_i r_i\right) \quad (4.2)$$

Due to the algorithmic similarity to the sampling of the soft-thresholded Gaussian process model to be presented in the numerical experiments, we omit further detail on the sampling for latent Gaussian models.

The second extension is on the sampling of truncated multivariate Gaussian:

$$\Pi(\theta | \mu, \Sigma, R) \propto \exp \left[-\frac{1}{2} (\theta - \mu)^T \Sigma^{-1} (\theta - \mu) \right] 1(\theta \in R) \quad (4.3)$$

where $\mu \in \mathbb{R}^p$, Σ is positive definite, and R some constrained set of dimension p . Despite being commonality in statistical application, the truncated multivariate Gaussian can pose a challenge for sampling, especially in high dimension (Wilhelm and Manjunath, 2010; Chow and Saad, 2014), due to having correlation and truncation at the same time. Using the anti-correlation Gaussian

$(r \mid \theta, \mu, \Sigma) \sim N[(dI - \Sigma^{-1})(\theta - \mu), dI - \Sigma^{-1}]$, we have

$$\Pi(\theta \mid \mu, r) \propto 1(\theta \in R) \prod_{j=1}^p \exp[-\frac{1}{2}d(\theta_j - \mu_j)^2 + (\theta_j - \mu_j)r_j]. \quad (4.4)$$

When the constraints in R are separable over each sub-dimension, then θ_j is conditionally independent over j . For example, with simple box constraint $R = \cap_{j=1}^p \{x : l_j < x_j < r_j\}$, then each θ_j follows a univariate truncated Gaussian and θ can be sampled in a block. We give a numerical example in Appendix B.4.

5 Numerical Examples

We now use several numerical examples to show the computational efficiency of the anti-correlation blocked Gibbs sampler.

5.1 Linear Regression

We first consider the setting where M is non-diagonal. We use linear regression with $y_i \sim N(x_i^T \theta, \sigma^2)$, $x_i \in \mathbb{R}^p$ simulated from a multivariate Gaussian with mean zero, and correlation $\rho^{|j-j'|}$ between $x_{i,j}$ and $x_{i,j'}$. During data generation, in each experiment, we set the ground truth $\sigma^2 = 1$ and θ as one of the vectors from a range of signal-to-noise ratios, as previously used by Yang et al. (2016). Specifically, we set the first 10 elements of θ to

$$c \sqrt{\frac{\sigma^2 \log(p)}{n}} (2, -3, 2, 2, -3, 3, -2, 3, -2, 3)^T,$$

where c is the selected signal-to-noise ratio, taken from $\{1, 2, 3, 6\}$, with $c = 1$ in a low-to-moderate signal regime, and $c \geq 2$ in a strong signal regime (Yang et al., 2016). The other elements of θ are set to zero. For the prior specification, we use $\beta_j \stackrel{\text{indep}}{\sim} N(0, \tau_j)$, with $\tau_j \sim \text{Inverse-Gamma}(a_j, b_j)$, and $\kappa_0 \sim \text{Exp}(\lambda)$ (we use rate parameterization for all inverse-gamma and exponential distributions). We choose the exponential prior for λ as a weakly-informative prior, so that the κ_0 should be relatively small as a priori, while the light tail of exponential allows the posterior to have potentially large κ_0 . For the noise variance, we use $\sigma^2 \sim \text{Inverse-Gamma}(a_\sigma, b_\sigma)$. In the experiments, we use $n = 300$, $p \in \{10, 50, 500\}$, $\rho \in \{0.5, 0.9\}$, $a_j = 5$, $b_j = 1$, $a_\sigma = 1$, $b_\sigma = 1$ and $\lambda = 1$.

For benchmarking, we compare our algorithm against three other samplers: (i) the No-U-Turn (NUTS) sampler (Hoffman and Gelman, 2014); (ii) the component-wise slice sampler (Neal, 2003) that updates one element at a time; (iii) the empirical principal component-based slice sampler (Thompson, 2011) with randomized directions. To provide more details about (iii), we use an empirical estimate of the covariance between all parameters (based on running 200 iterations of the component-wise slice sampler during an adaptation period, and the adaptation time cost is excluded from the calculation of computing efficiency), take the first 10 principal components, and run the slice sampler along each direction under slight perturbation (by adding Gaussian noise $N(0, 1/4p)$ to each element of direction, then rescaling the perturbed direction vector to have unit 2-norm). For (ii) and (iii), we use the stepping out and shrinkage procedures (Neal, 2003) to draw a subset of slices.

We conduct 10 times of repeated experiments under each setting, with different random seed numbers. At $\rho = 0.5$, we run MCMC for 10,000 iterations, and treat the first 2,000 as burn-ins; at $\rho = 0.9$, since the high pairwise correlation slightly slows down the mixing, we run MCMC for 20,000 iterations, and treat the first 10,000 as burn-ins. We record the total wall clock time (in seconds), and calculate the effective sample size. Since the popular NUTS sampler implementation, Stan (Carpenter et al., 2017) is coded in C++, while all the other three algorithms are done in R, to have a fair comparison of the algorithmic efficiency, we estimate the running time of NUTS using a pure R implementation from the ‘hmclearn’ package (Thomas and Tu, 2021). Specifically, we first obtain the total number of leap-frog steps from the diagnostics of Stan program, then run the same number of leap-frog steps in ‘hmclearn’ and record wall clock time.

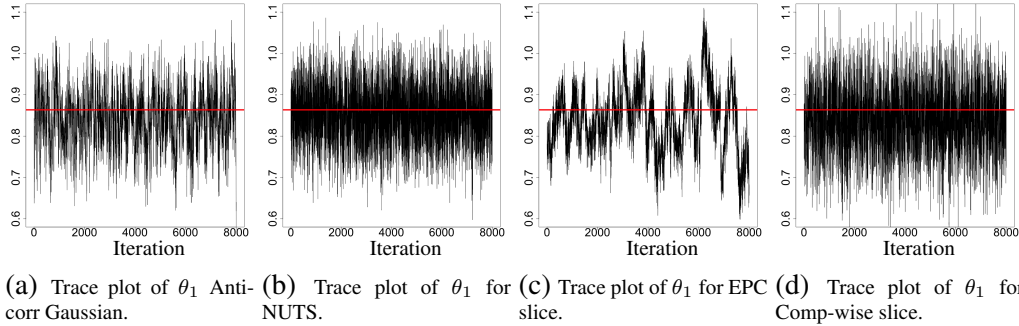


Figure 1: Trace plots for the four algorithms: anti-correlation Gaussian (Anti-corr Gaussian), No-U-Turn Sampler (NUTS), empirical principal component-based slice sampler (EPC slice), and component-wise slice sampler (Comp-wise slice). The horizontal lines are the ground truth.

To compare the algorithms in terms of variable selection and estimation accuracy, we report the false positive rates (FPR), false negative rates (FNR) and mean squared errors (MSE) for estimating regression coefficients θ in Tables 1 and 2. The FPR and FNR are computed based on the element-wise 95% credible intervals of θ_j 's. The FPR is the proportion of the intervals corresponding to the ground truth zero that do not cover zero, while the FNR is the proportion of the intervals corresponding to the non-zero ground truth that cover zero. When $c = 1$, the signal is not strong, and all algorithms fail to produce good results. At $\rho = 0.9$, the correlations within the design matrix are strong, and anti-correlation blocked Gibbs sampler outperforms all the other algorithms. At $\rho = 0.5$ and $c \geq 2$, the anti-correlation Gaussian, the NUTS, and the component-wise slice sampler work similarly well, while the EPC slice sampler gives bad results when $p = 500$. We find similar results in MSE.

		$c = 1$	$c = 2$	$c = 3$	$c = 6$
		FPR,FNR	FPR,FNR	FPR,FNR	FPR,FNR
$p = 10, \rho = 0.5$	Anti-corr Gaussian	-, 65	-, 2	-, 0	-, 0
	NUTS	-, 49	-, 0	-, 0	-, 0
	Comp-wise slice	-, 96	-, 7	-, 0	-, 0
	EPC slice	-, 56	-, 6	-, 0	-, 0
$p = 50, \rho = 0.5$	Anti-corr Gaussian	0, 67	0, 0	0, 0	0, 0
	NUTS	0, 71	0, 1	0, 0	0, 0
	Comp-wise slice	0, 87	0, 5	0, 0	0, 0
	EPC slice	0, 79	0, 0	0, 0	0, 0
$p = 500, \rho = 0.5$	Anti-corr Gaussian	0, 65	0, 0	0, 0	0, 0
	NUTS	0, 72	0, 0	0, 0	0, 0
	Comp-wise slice	0, 87	0, 0	0, 0	0, 0
	EPC slice	0, 95	0, 81	0, 52	0, 23
$p = 10, \rho = 0.9$	Anti-corr Gaussian	-, 100	-, 55	-, 0	-, 0
	NUTS	-, 99	-, 69	-, 31	-, 0
	Comp-wise slice	-, 100	-, 100	-, 94	-, 73
	EPC slice	-, 98	-, 64	-, 21	-, 0
$p = 50, \rho = 0.9$	Anti-corr Gaussian	0, 94	0, 74	0, 0	0, 0
	NUTS	0, 100	0, 87	0, 49	0, 0
	Comp-wise slice	0, 98	0, 95	0, 89	0, 60
	EPC slice	0, 89	1, 80	2, 39	3, 5
$p = 500, \rho = 0.9$	Anti-corr Gaussian	0, 86	0, 77	0, 0	0, 0
	NUTS	0, 96	0, 85	0, 20	0, 0
	Comp-wise slice	0, 90	0, 90	0, 60	0, 50
	EPC slice	0, 87	0, 82	0, 81	0, 75

Table 1: False positive rates (FPR) and false negative rates (FNR) (measured in %) for the four algorithms: anti-correlation Gaussian (Anti-corr Gaussian), No-U-Turn Sampler (NUTS), empirical principal component-based slice sampler (EPC slice), and component-wise slice sampler (Comp-wise slice). When $p = 10$, there is no FPR as all ground-truth θ_j 's are non-zero.

		$c = 1$	$c = 2$	$c = 3$	$c = 6$
$p = 10, \rho = 0.5$	Anti-corr Gaussian	0.0082	0.0056	0.0058	0.0063
	NUTS	0.0078	0.0042	0.0067	0.0059
	Comp-wise slice	0.0192	0.0045	0.0047	0.0067
	EPC slice	0.0118	0.0072	0.0092	0.0054
$p = 50, \rho = 0.5$	Anti-corr Gaussian	0.0041	0.0018	0.0015	0.0017
	NUTS	0.0057	0.0013	0.0014	0.0013
	Comp-wise slice	0.0053	0.0014	0.0016	0.0016
	EPC slice	0.0101	0.0021	0.0020	0.0018
$p = 500, \rho = 0.5$	Anti-corr Gaussian	0.0009	0.0002	0.0002	0.0001
	NUTS	0.0009	0.0002	0.0002	0.0001
	Comp-wise slice	0.0025	0.0003	0.0001	0.0003
	EPC slice	0.0026	0.0087	0.0126	0.0217
$p = 10, \rho = 0.9$	Anti-corr Gaussian	0.0379	0.0358	0.0597	0.0810
	NUTS	0.0329	0.0515	0.0561	0.0628
	Comp-wise slice	0.0402	0.1270	0.2410	0.3436
	EPC slice	0.0351	0.0572	0.0498	0.0791
$p = 50, \rho = 0.9$	Anti-corr Gaussian	0.0150	0.0310	0.0217	0.0216
	NUTS	0.0137	0.0249	0.0262	0.0183
	Comp-wise slice	0.0144	0.0489	0.0886	0.1316
	EPC slice	0.0140	0.0458	0.0578	0.0516
$p = 500, \rho = 0.9$	Anti-corr Gaussian	0.0023	0.0074	0.0014	0.0020
	NUTS	0.0019	0.0068	0.0009	0.0005
	Comp-wise slice	0.0024	0.0082	0.0128	0.0116
	EPC slice	0.0025	0.0099	0.0210	0.0742

Table 2: Mean squared error (MSE) for estimating θ via the four algorithms under different settings.

At $c = 3$ and $\rho = 0.5$, we report in Table 3 the average running time for 1,000 iterations. The anti-correlation Gaussian is the fastest, followed by EPC slice, component-wise slice, and NUTS. As shown in Figure 1, the NUTS algorithm has the fastest mixing; however, this is at the cost of expensive computation per iteration. To further illustrate the advantage of the anti-correlation blocked Gibbs sampler in terms of computational efficiency, we compare the effective sample size per computing time in Table 4. It can be seen that the anti-correlation Gaussian has the highest effective sample size per computing time.

p	Anti-corr Gaussian	NUTS	Comp-wise slice	EPC slice
10	0.41	26.18	3.61	3.04
50	0.93	108.33	31.44	4.16
500	5.60	22875.74	1121.47	16.14

Table 3: Running time for 1,000 iterations for the four algorithms. The time unit is in seconds based on pure R implementation for each algorithm.

(p, ρ)	Anti-corr Gaussian	NUTS	Comp-wise slice	EPC slice
(10, 0.5)	202.36, 265.56	8.82, 7.05	49.08, 60.31	5.19, 8.23
(50, 0.5)	62.86, 165.74	1.52, 2.46	5.12, 4.61	4.34, 5.98
(500, 0.5)	4.81, 34.95	0.01, 0.01	0.10, 0.14	2.36, 7.58
(10, 0.9)	31.19, 35.79	4.22, 3.89	No convergence	3.61, 4.48
(50, 0.9)	11.28, 15.18	0.53, 1.05	No convergence	No convergence
(500, 0.9)	3.05, 14.50	<0.01, <0.01	No convergence	No convergence

Table 4: Effective sample size per computing time (ESS/s) for the four algorithms. In each cell, the first number is the average ESS/s for the first 10 entries, and the second number is the average ESS/s for the rest entries. Each ESS/s is reported as the average result of 10 repetitions with a different seed number. The two slice samplers fail to converge to the ground truth in some settings within 20,000 iterations.

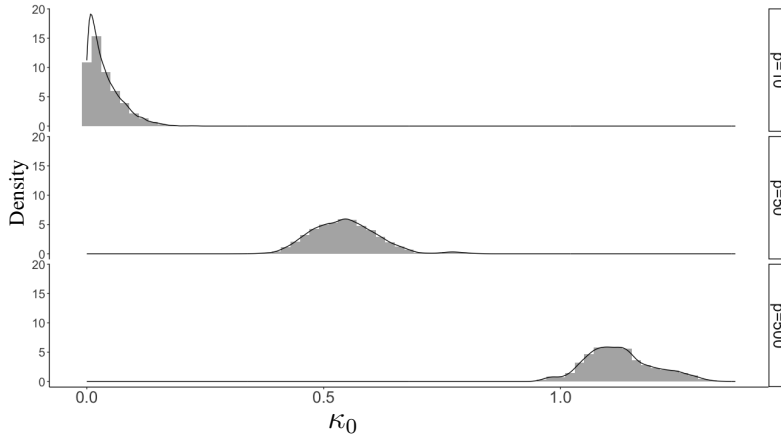


Figure 2: Posterior density estimations of κ_0 for varying dimensions p when $(c, \rho) = (3, 0.5)$.

Figure 2 shows the posterior distribution of κ_0 under different values of p . As p increases, the mode of the posterior density of κ_0 increases, as a result of the higher level of sparsity.

5.2 Application on Soft-Thresholded Gaussian Process

We next focus on the setting with non-diagonal H . We consider an application of the soft-thresholded Gaussian process (Kang et al., 2018):

$$\theta_s = \text{sign}(\beta_s) \circ (|\beta_s| - \kappa_0)_+, \quad \beta \sim \text{GP}[0, K(\cdot, \cdot)],$$

where s is the location in some input location space \mathbb{S} , $\kappa_0 > 0$ is a scalar, and GP denotes a Gaussian process from which any finite-dimensional realization follows a multivariate (potentially degenerate) Gaussian with zero mean, and covariance parameterized by $\text{Cov}(\beta_s, \beta_{s'}) = K(s, s')$. With an appropriate choice of K , we can obtain useful properties on a GP realization, such as continuity or smoothness over s . After applying soft-thresholding, we preserve the continuity over \mathbb{S} , and smoothness in each open set where $\theta_s \neq 0$. Therefore, the above is useful for obtaining a “smooth *and* sparse” parameterization for θ . In this article, we consider a simple but useful application in image smoothing, in the form of:

$$y_s = \theta_s + \epsilon_s, \quad \epsilon_s \stackrel{iid}{\sim} \text{N}(0, \sigma^2),$$

where s is the pixel location, $s = (i, j)$ with $i = 1, \dots, n_1$ and $j = 1, \dots, n_2$. We set the covariance function as $K(s, s') = \tau \exp[-\|s - s'\|_2^2 / (2\xi^2)]$.

In application, we use the functional magnetic resonance imaging scan of one human subject who was performing a motor task. We take a sectional view along the anterior-posterior axis of the brain, corresponding to 91×91 pixels per frame, and over a time period, we collect 280 frames. Using superscript f to index each frame, we assume $y^f = \{y_s^f\}_{\text{all } s}$ to be independent over f with frame-varying mean $\theta^f = \{\theta_s^f\}_{\text{all } s}$, but the other parameters σ^2 , τ , ξ and κ_0 are invariant over $f = 1, \dots, 280$. To finish the prior specification, we use $\tau \sim \text{Inverse-Gamma}(0.1, 0.1)$, $\sigma^2 \sim \text{Inverse-Gamma}(0.1, 0.1)$ and $\kappa_0 \sim \text{Exp}(0.5)$. Tikhonov et al. (2020) has previously shown that when the goal of using GP is to obtain smoothing of data, estimating the bandwidth ξ under a reasonable degree of precision is empirically adequate. Specifically, they impose a simple discrete prior on ξ supported on a finite set of values, so that all possible precision matrix H and its determinant could be pre-computed, hence further facilitating the computation. We follow

their solution here, with $\xi = 0.5\tilde{t}$ and \tilde{t} a discrete uniform prior supported on $\{1, \dots, 20\}$.

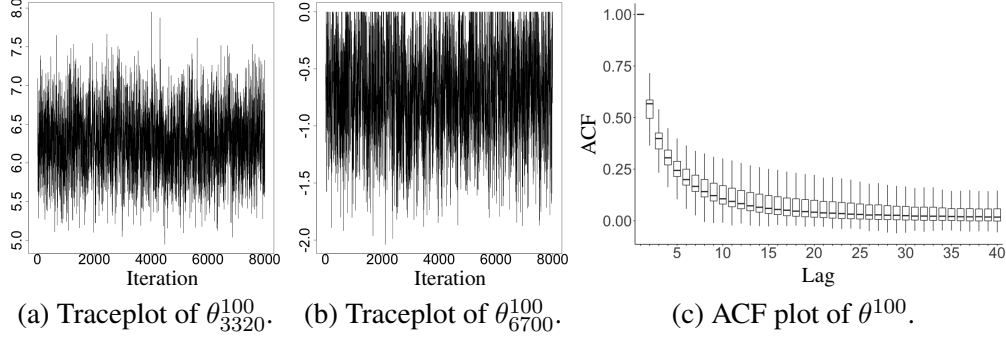


Figure 3: Trace plots and autocorrelation function (ACF) plot. Each box on the ACF plot incorporates the ACF for all pixels of an image.

When using our proposed Gibbs sampler for posterior estimation, we sample β using the anti-correlation Gaussian data augmentation technique, sample σ^2 and τ from their corresponding inverse-gamma full conditional distributions, and sample each of ξ and κ_0 using the slice sampling algorithm. We run 10,000 iterations with the first 2,000 as burn-ins, and it takes about 270 minutes on a MacBook Pro with a 10-core CPU. We report the effective sample size per hour for four randomly selected locations of θ^{100} at $f = 100$: 315.14 at $s = 3300$, 315.44 at $s = 3320$, 268.95 at $s = 3720$, and 227.16 at $s = 6700$. To further assess the mixing, we plot both the trace plots at two locations and an autocorrelation function (ACF) plot in Figure 3. The trace plots show fast mixing and the ACF drops quickly.

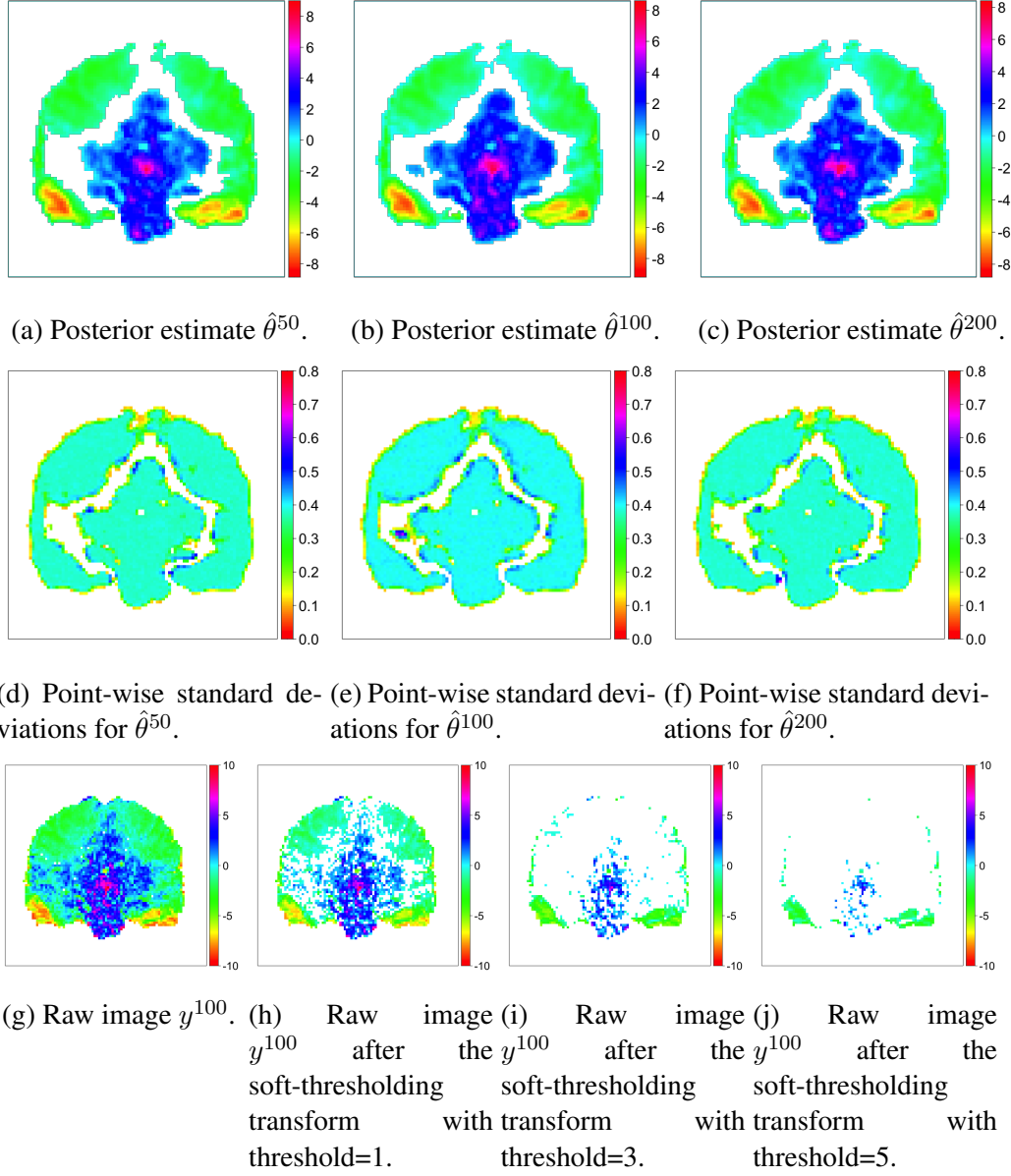


Figure 4: Posterior estimates, point-wise standard deviations, and direct soft-thresholding transform on a raw image. The posterior estimates by soft-thresholded GP are smooth and sparse with point-wise uncertainty estimated whereas the direct soft-thresholding transform only leads to noisy estimates.

In Figure 4, images (a)-(c) show the posterior mean estimates for three frames,

and images (d)-(f) give the point-wise standard deviations. We can clearly see both smoothness and sparsity in the mean estimates, as well as how they change over time. To show the benefits of using a soft-thresholded GP, we also plot the results of simple thresholding on the raw images in (g)-(j), which lead to non-smooth estimates and scattered noisy non-zero points on the estimates.

To show how our proposed algorithm improves the computational efficiency of the soft-thresholded GP method, we also run a No-U-Turn sampler on the same model using Stan. We try NUTS with max tree depth equal to 7, it takes 68 hours to finish 10,000 iterations, and the effective sample size per hour for estimating θ^{100} is 8.1 on average, 9.2 at $s = 3300$, 9.3 at $s = 3320$, 7.4 at $s = 3720$, and 6.7 at $s = 6700$. Therefore, our algorithm improves the computing speed substantially.

6 Discussion

The latent Gaussian form is very common in Bayesian posterior estimation. In this article, we show the advantages of using anti-correlation Gaussian to cancel out the quadratic term in the exponent. We expect our technique to be broadly applicable beyond our presented scenarios. For example, one could potentially extend this technique to address sampling problems of Bingham distribution in Stiefel manifold (Hoff, 2009), the costly evaluation of determinant in determinantal point process (Kulesza et al., 2012), and so forth.

When it comes to linear regression variable selection using discrete spike-and-slab prior, there is some close connection of our algorithm to the ODA algorithm (Ghosh and Clyde, 2011), which uses an augmented design matrix to make the complete gram matrix diagonal. Since one could reparameterize a discrete spike-and-slab prior as a special case of the L1-ball prior by setting κ according to a quantile of $\pi_0(\beta)$, we expect our geometric ergodicity result could be extended to analyzing the ODA algorithm. In comparison, our algorithm has the advantages of not having to create an augmented design matrix and easy application in non-linear models. We expect some nice properties that are further exploited in the ODA algorithm, such as the collapsed sampling step based on marginalizing out θ_j given if $b_j = 1$ or 0, could be obtained in some specific form of latent Gaussian model after we augment the anti-correlation Gaussian.

References

- Albert, J. H. and S. Chib (1993). Bayesian Analysis of Binary and Polychotomous Response Data. *Journal of the American Statistical Association* 88(422), 669–679. 2, 8
- Armagan, A., D. B. Dunson, and J. Lee (2013). Generalized Double Pareto Shrinkage. *Statistica Sinica* 23(1), 119. 2
- Bai, R. and M. Ghosh (2019). On the Beta Prime Prior for Scale Parameters in High-Dimensional Bayesian Regression Models. *Statistica Sinica*. 2
- Betancourt, B., A. Rodríguez, and N. Boyd (2017). Bayesian Fused Lasso Regression for Dynamic Binary Networks. *Journal of Computational and Graphical Statistics* 26(4), 840–850. 3
- Bhattacharya, A., A. Chakraborty, and B. K. Mallick (2016). Fast Sampling With Gaussian Scale Mixture Priors in High-Dimensional Regression. *Biometrika* 103(4), 985–991. 8
- Bhattacharya, A., D. Pati, N. S. Pillai, and D. B. Dunson (2015). Dirichlet–Laplace Priors for Optimal Shrinkage. *Journal of the American Statistical Association* 110(512), 1479–1490. 2
- Bingham, E., J. P. Chen, M. Jankowiak, F. Obermeyer, N. Pradhan, T. Karaletos, R. Singh, P. A. Szerlip, P. Horsfall, and N. D. Goodman (2019). Pyro: Deep Universal Probabilistic Programming. *Journal of Machine Learning Research* 20, 28:1–28:6. 4
- Bottolo, L. and S. Richardson (2010). Evolutionary Stochastic Search for Bayesian Model Exploration. *Bayesian Analysis* 5(3), 583–618. 2
- Carpenter, B., A. Gelman, M. D. Hoffman, D. Lee, B. Goodrich, M. Betancourt, M. A. Brubaker, J. Guo, P. Li, and A. Riddell (2017). Stan: A Probabilistic Programming Language. *Journal of Statistical Software* 76. 4, 14
- Carvalho, C. M., N. G. Polson, and J. G. Scott (2010). The Horseshoe Estimator for Sparse Signals. *Biometrika* 97(2), 465–480. 2
- Chandra, N. K., P. Mueller, and A. Sarkar (2021). Bayesian Scalable Precision Factor Analysis for Massive Sparse Gaussian Graphical Models. *arXiv Preprint arXiv:2107.11316*. 9

- Chow, E. and Y. Saad (2014). Preconditioned Krylov Subspace Methods for Sampling Multivariate Gaussian Distributions. *SIAM Journal on Scientific Computing* 36(2), A588–A608. 12
- Diaconis, P., K. Khare, and L. Saloff-Coste (2008). Gibbs Sampling, Exponential Families and Orthogonal Polynomials. *Quality Engineering* 54, 31–32. 11
- Duane, S., A. D. Kennedy, B. J. Pendleton, and D. Roweth (1987). Hybrid Monte Carlo. *Physics Letters B* 195(2), 216–222. 3
- Fahrmeir, L. and G. Tutz (2001). *Multivariate Statistical Modelling Based on Generalized Linear Models*. Springer Series in Statistics. Springer New York. 12
- Gelman, A. (2014). *Bayesian Data Analysis* (Third edition ed.). Chapman & Hall/CRC texts in statistical science. CRC Press. 12
- George, E. I. and R. E. McCulloch (1995). Stochastic Search Variable Selection. *Markov Chain Monte Carlo in Practice* 68, 203–214. 2, 37
- Ghosh, J. and M. A. Clyde (2011). Rao–Blackwellization for Bayesian Variable Selection and Model Averaging in Linear and Binary Regression: A Novel Data Augmentation Approach. *Journal of the American Statistical Association* 106(495), 1041–1052. 2, 22
- Ghosh, J. and D. B. Dunson (2009). Default Prior Distributions and Efficient Posterior Computation in Bayesian Factor Analysis. *Journal of Computational and Graphical Statistics* 18(2), 306–320. 9
- Girolami, M. and B. Calderhead (2011). Riemann Manifold Langevin and Hamiltonian Monte Carlo Methods. *Journal of the Royal Statistical Society Series B: Statistical Methodology* 73(2), 123–214. 3
- Griffin, M. and P. D. Hoff (2023). Structured Shrinkage Priors. *Journal of Computational and Graphical Statistics* (in press), 1–22. 2
- Hans, C., A. Dobra, and M. West (2007). Shotgun Stochastic Search for “Large P” Regression. *Journal of the American Statistical Association* 102(478), 507–516. 2

- Hoff, P. D. (2009). Simulation of the Matrix Bingham–Von Mises–Fisher Distribution, With Applications to Multivariate and Relational Data. *Journal of Computational and Graphical Statistics* 18(2), 438–456. 22
- Hoff, P. D. (2017). Lasso, Fractional Norm and Structured Sparse Estimation Using a Hadamard Product Parametrization. *Computational Statistics & Data Analysis* 115, 186–198. 2
- Hoffman, M. D. and A. Gelman (2014). The No-U-Turn Sampler: Adaptively Setting Path Lengths in Hamiltonian Monte Carlo. *Journal of Machine Learning Research* 15(1), 1593–1623. 3, 4, 14
- Kang, J., B. J. Reich, and A.-M. Staicu (2018). Scalar-on-Image Regression via the Soft-Thresholded Gaussian Process. *Biometrika* 105(1), 165–184. 3, 19, 34
- Kulesza, A., B. Taskar, et al. (2012). Determinantal Point Processes for MacHine Learning. *Foundations and Trends in Machine Learning* 5(2–3), 123–286. 22
- Kwon, D., M. T. Landi, M. Vannucci, H. J. Issaq, D. Prieto, and R. M. Pfeiffer (2011). An Efficient Stochastic Search for Bayesian Variable Selection With High-Dimensional Correlated Predictors. *Computational Statistics & Data Analysis* 55(10), 2807–2818. 2
- Liu, J. S., W. H. Wong, and A. Kong (1994). Covariance Structure of the Gibbs Sampler With Applications to the Comparisons of Estimators and Augmentation Schemes. *Biometrika* 81(1), 27–40. 11
- Livingstone, S. and G. Zanella (2022). The Barker Proposal: Combining Robustness and Efficiency in Gradient-Based McMc. *Journal of the Royal Statistical Society Series B: Statistical Methodology* 84(2), 496–523. 3
- Meyn, S. P. and R. L. Tweedie (1994). Computable Bounds for Geometric Convergence Rates of Markov Chains. *The Annals of Applied Probability* 4(4), 981–1011. 28
- Mitchell, T. J. and J. J. Beauchamp (1988). Bayesian Variable Selection in Linear Regression. *Journal of the American Statistical Association* 83(404), 1023–1032. 2
- Neal, R. M. (2003). Slice Sampling. *The Annals of Statistics* 31(3), 705–767. 14

- Neal, R. M. (2011). MCMC Using Hamiltonian Dynamics. In S. Brooks, A. Gelman, G. Jones, and X.-L. Meng (Eds.), *Handbook of Markov Chain Monte Carlo*, Chapter 5. CRC Press. 4
- Nishimura, A. and M. A. Suchard (2022). Prior-Preconditioned Conjugate Gradient Method for Accelerated Gibbs Sampling in “Large N, Large P” Bayesian Sparse Regression. *Journal of the American Statistical Association*, 1–14. 8
- Piironen, J. and A. Vehtari (2017). Sparsity Information and Regularization in the Horseshoe and Other Shrinkage Priors. *Electronic Journal of Statistics* 11(2), 5018–5051. 2
- Polson, N. G. and J. G. Scott (2010). Shrink Globally, Act Locally: Sparse Bayesian Regularization and Prediction. *Bayesian Statistics* 9(501-538), 105. 2
- Polson, N. G., J. G. Scott, and J. Windle (2013). Bayesian Inference for Logistic Models Using Pólya–Gamma Latent Variables. *Journal of the American Statistical Association* 108(504), 1339–1349. 5
- Qin, Q., J. P. Hobert, and K. Khare (2019). Estimating the Spectral Gap of A Trace-Class Markov Operator. *Electronic Journal of Statistics* 13(1), 1790 – 1822. 11
- Robert, C. P. (1995). Convergence Control Methods for Markov Chain Monte Carlo Algorithms. *Statistical Science* 10(3), 231–253. 11
- Robert, C. P. and G. Casella (2004). *Monte Carlo Statistical Methods* (2nd ed ed.). Springer texts in statistics. New York: Springer. 12
- Roberts, G. O. and J. S. Rosenthal (2001). Markov Chains and De-Initializing Processes. *Scandinavian Journal of Statistics* 28(3), 489–504. 11
- Rocková, V. and E. I. George (2018). The Spike-and-Slab Lasso. *Journal of the American Statistical Association* 113(521), 431–444. 2
- Rosenthal, J. S. (1994). Minorization Conditions and Convergence Rates for Markov Chain Monte Carlo. *Journal of the American Statistical Association* 90, 558–566. 28

- Rossky, P. J., J. D. Doll, and H. L. Friedman (1978). Brownian Dynamics as Smart Monte Carlo Simulation. *The Journal of Chemical Physics* 69(10), 4628–4633. 4
- Rue, H., S. Martino, and N. Chopin (2009). Approximate Bayesian Inference for Latent Gaussian Models by Using Integrated Nested Laplace Approximations. *Journal of the Royal Statistical Society Series B: Statistical Methodology* 71(2), 319–392. 12
- Scott, S. L. and H. R. Varian (2014). Predicting the Present With Bayesian Structural Time Series. *International Journal of Mathematical Modelling and Numerical Optimisation* 5(1-2), 4–23. 37
- Tadesse, M. G. and M. Vannucci (2021). *Handbook of Bayesian Variable Selection*. CRC Press. 2
- Tan, A., G. L. Jones, and J. P. Hobert (2013, January). On the Geometric Ergodicity of Two-Variable Gibbs Samplers. In *Advances in Modern Statistical Theory and Applications: A Festschrift in honor of Morris L. Eaton*, Volume 10, pp. 25–43. Institute of Mathematical Statistics. 10
- Thomas, S. and W. Tu (2021). Learning Hamiltonian Monte Carlo in R. *The American Statistician* 75(4), 403–413. 14
- Thompson, M. (2011). *Slice Sampling With Multivariate Steps*. University of Toronto Toronto, Canada. 14
- Tibshirani, R., M. Saunders, S. Rosset, J. Zhu, and K. Knight (2005). Sparsity and Smoothness via the Fused Lasso. *Journal of the Royal Statistical Society: Series B (Statistical Methodology)* 67(1), 91–108. 3
- Tikhonov, G., Ø. H. Opedal, N. Abrego, A. Lehikoinen, M. M. de Jonge, J. Oksanen, and O. Ovaskainen (2020). Joint Species Distribution Modelling With the R-Package Hmsc. *Methods in Ecology and Evolution* 11(3), 442–447. 19
- Wilhelm, S. and B. Manjunath, G. (2010). tmvtnorm: A Package for the Truncated Multivariate Normal Distribution. *The R Journal* 2(1), 25. 12, 36
- Xu, M. and L. L. Duan (2023). Bayesian Inference With the L1-Ball Prior: Solving Combinatorial Problems With Exact Zeros. *Journal of the Royal Statistical Society: Series B (Statistical Methodology)* (in press). 3

Yang, Y., M. J. Wainwright, and M. I. Jordan (2016). On the Computational Complexity of High-Dimensional Bayesian Variable Selection. *The Annals of Statistics* 44(6), 2497–2532. [2](#), [13](#)

A Proof of Geometric Ergodicity in Linear Models

We wish to prove the geometric ergodicity of the Markov chain $\{r^k, t^k\}_{k=0}^\infty$. To ease the burden of notation, we denote (r^0, t^0) the current state and (r, t) the next state generated by first sampling $(\theta, \beta)|(r, t)$ according to (2.5) and (2.6) and then sampling $(r, t)|(\theta, \beta)$ according to (2.2). Let $\|\cdot\|$ denote the Euclidean norm and define $V(x, y) := \|x + y\|^2$ for any $x, y \in \mathbb{R}^p$. Invoking Theorem 12 in [Rosenthal \(1994\)](#) (See also [Meyn and Tweedie \(1994\)](#)), it suffices to show the following two conditions hold:

1. **Drift condition:** There exist $\tilde{\lambda} < 1$ and $\tilde{b} < \infty$ such that $\mathbb{E}[V(r, t)|r^0, t^0] \leq \tilde{\lambda}V(r^0, t^0) + \tilde{b}$ for any $(r^0, t^0) \in \mathbb{R}^{2p}$.
2. **Minorization condition:** For some $\tilde{d} > 2\tilde{b}/(1 - \tilde{\lambda})$, there exist $\varepsilon > 0$ and a probability measure $Q : \mathbb{R}^p \times \mathbb{R}^p \rightarrow \mathbb{R}$ such that $P_{r,t}((r^0, t^0), \cdot) \geq \varepsilon Q(\cdot)$ holds for all $(r^0, t^0) \in \mathbb{R}^{2p}$ satisfying $V(r^0, t^0) \leq \tilde{d}$.

1. Drift condition: It is known that for a random variable X following a truncated Gaussian distribution $N_{(a,b)}(\mu, \sigma^2)$, we have $\mathbb{E}[X] = \mu + \frac{\varphi(\alpha) - \varphi(\beta)}{\Phi(\beta) - \Phi(\alpha)}\sigma$ where $\alpha = (a - \mu)/\sigma$, $\beta = (b - \mu)/\sigma$, $\varphi(\cdot)$ is the probability density function of the standard Gaussian distribution and $\Phi(\cdot)$ is its cumulative distribution function. Besides, because the truncation reduces the variance, it follows that $\text{Var}(X) \leq \sigma^2$. Hence, we can derive an upper bound for the second moment of X :

$$\mathbb{E}[X^2] \leq \left(\mu + \frac{\varphi(\alpha) - \varphi(\beta)}{\Phi(\beta) - \Phi(\alpha)}\sigma \right)^2 + \sigma^2. \quad (\text{A.1})$$

It follows that for any $j = 1, \dots, p$,

$$\mathbb{E}[\beta_j^2 | b_j = 1, r^0, t^0] \leq \left(\mu_j^0 + \frac{\varphi(\frac{\kappa_j - \mu_j^0}{\sigma})}{1 - \Phi(\frac{\kappa_j - \mu_j^0}{\sigma})}\sigma \right)^2 + \sigma^2 := \zeta_j^0,$$

where $\mu_j^0 = \frac{\phi_j + r_j^0 + \psi_j + t_j^0 + d\kappa_j}{d+e}$ and $\sigma = \frac{1}{\sqrt{d+e}}$.

Using the asymptotic property of the Mill's ratio $\lim_{x \rightarrow +\infty} \frac{\varphi(x)}{x(1-\Phi(x))} = 1$ and $\lim_{x \rightarrow -\infty} \frac{\varphi(x)}{x(1-\Phi(x))} = 0$, we have

$$\lim_{\mu_j^0 \rightarrow +\infty} \frac{\zeta_j^0}{(\mu_j^0)^2} = 1, \text{ and } \lim_{\mu_j^0 \rightarrow -\infty} \frac{\zeta_j^0}{(\mu_j^0)^2} = 0.$$

Furthermore, in view of the fact that $\lim_{|r_j^0 + t_j^0| \rightarrow \infty} \frac{r_j^0 + t_j^0}{d+e} / \mu_j^0 = 1$, we get

$$\lim_{r_j^0 + t_j^0 \rightarrow +\infty} \frac{\zeta_j^0}{\left(\frac{r_j^0 + t_j^0}{d+e}\right)^2} = 1, \text{ and } \lim_{r_j^0 + t_j^0 \rightarrow -\infty} \frac{\zeta_j^0}{\left(\frac{r_j^0 + t_j^0}{d+e}\right)^2} = 0.$$

It follows that for any real number $q > 1$, there exists a real number $\tilde{C}_j > 0$, such that for all $(r_j^0, t_j^0) \in \mathbb{R}^2$,

$$\zeta_j^0 < q \left(\frac{r_j^0 + t_j^0}{d+e} \right)^2 + \tilde{C}_j.$$

In particular, one can take $q = \frac{1-\nu/2}{1-\nu}$ where $\nu := 1 - (\lambda_p(dI - M) + \lambda_p(eI - H))^2 / (d+e)^2 \in (0, 1)$ and $\lambda_p(A)$ denotes the largest eigenvalue of matrix A . Then we have

$$\zeta_j^0 < \frac{1-\nu/2}{1-\nu} \left(\frac{r_j^0 + t_j^0}{d+e} \right)^2 + \tilde{C}_j.$$

Noting that a similar result can be reached with a different constant term than \tilde{C}_j for when $b_j = -1$ is given, and that when $b_j = 0$ is given, $\beta_j^2 \leq \kappa_j^2$, we conclude that

$$\mathbb{E}[\beta_j^2 | b_j = i, r^0, t^0] \leq \frac{1-\nu/2}{1-\nu} \left(\frac{r_j^0 + t_j^0}{d+e} \right)^2 + C$$

for $i \in \{-1, 0, 1\}$, $j \in \{1, \dots, p\}$ and some constant C . Hence,

$$\begin{aligned}
\mathbb{E}[\|\beta\|^2 | r^0, t^0] &= \sum_{j=1}^p \mathbb{E}[\beta_j^2 | r^0, t^0] \\
&= \sum_{j=1}^p \sum_{i \in \{-1, 0, 1\}} \mathbb{E}[\beta_j^2 | b_j = i, r^0, t^0] \Pr(b_j = i | r^0, t^0) \\
&\leq \sum_{j=1}^p \left[\frac{1 - \nu/2}{1 - \nu} \left(\frac{r_j^0 + t_j^0}{d + e} \right)^2 + C \right] \\
&= \frac{1 - \nu/2}{1 - \nu} \frac{1}{(d + e)^2} \|r^0 + t^0\|^2 + pC.
\end{aligned} \tag{A.2}$$

Thus, we establish the drift condition as follows:

$$\begin{aligned}
&\mathbb{E}[V(r, t) | r^0, t^0] \\
&= \mathbb{E}[\mathbb{E}(V(r, t) | \theta, \beta) | r^0, t^0] \\
&= \mathbb{E}[\mathbb{E}(\|r\|^2 + \|t\|^2 + 2r't | \theta, \beta) | r^0, t^0] \\
&\stackrel{(a)}{=} \mathbb{E}[\|(dI - M)\theta\|^2 + \|(eI - H)\beta\|^2 + 2\theta'(dI - M)(eI - H)\beta | r^0, t^0] \\
&\quad + tr(dI - M) + tr(eI - H) + tr \left(\begin{pmatrix} O & I_p \\ I_p & O \end{pmatrix} \begin{pmatrix} dI - M & O \\ O & eI - H \end{pmatrix} \right) \\
&\stackrel{(b)}{\leq} \lambda_p^2(dI - M) \mathbb{E}[\|\theta\|^2 | r^0, t^0] + \lambda_p^2(eI - H) \mathbb{E}[\|\beta\|^2 | r^0, t^0] \\
&\quad + 2\lambda_p(dI - M)\lambda_p(eI - H) \mathbb{E}[\|\theta\| \|\beta\| | r^0, t^0] + C' \\
&\stackrel{(c)}{\leq} (\lambda_p(dI - M) + \lambda_p(eI - H))^2 \mathbb{E}[\|\beta\|^2 | r^0, t^0] + C' \\
&\stackrel{(d)}{\leq} (\lambda_p(dI - M) + \lambda_p(eI - H))^2 \left[\frac{1 - \nu/2}{1 - \nu} \frac{1}{(d + e)^2} \|r^0 + t^0\|^2 + pC \right] + C' \\
&= \tilde{\lambda}V(r^0, t^0) + \tilde{b}
\end{aligned}$$

where $C' = tr(dI - M + eI - H)$, $\tilde{\lambda} = \frac{1 - \nu/2}{1 - \nu} \frac{(\lambda_p(dI - M) + \lambda_p(eI - H))^2}{(d + e)^2} = 1 - \frac{\nu}{2} \in (0, 1)$, and $\tilde{b} = C' + (\lambda_p(dI - M) + \lambda_p(eI - H))^2 pC < \infty$. (a) uses the fact that $(r, t) | (\theta, \beta)$ follows $2p$ -dimensional multivariate Gaussian distribution; (b) invokes the Rayleigh-Ritz theorem and for the third term, the Cauchy-Schwarz inequality; (c) uses the fact that $|\theta_j| = (|\beta_j| - \kappa_j)_+ \leq |\beta_j|$; (d) uses (A.2).

2. Minorization condition: Let $\pi(r, t | r^0, t^0)$ denote the probability density of (r, t) given the last state (r^0, t^0) by first drawing (θ, β) from $\pi(\theta, \beta | r^0, t^0)$ and

then drawing (r, t) from $\pi(r, t|\theta, \beta)$. For any $\tilde{d} > 0$, define the level set $\mathcal{G}_{\tilde{d}} := \{(r^0, t^0) \in \mathbb{R}^{2p} : V(r^0, t^0) \leq \tilde{d}\}$.

For all $(r^0, t^0) \in \mathcal{G}_{\tilde{d}}$, we have $|r_j^0 + t_j^0| < \sqrt{\tilde{d}}$ for any $j = 1, \dots, p$.

Note that

$$\begin{aligned}
& \pi(r, t|r^0, t^0) \\
&= \mathbb{E}_{(\theta, \beta|r^0, t^0)} [\pi(r, t|\theta, \beta)] \\
&= K_1 \mathbb{E}_{(\theta, \beta|r^0, t^0)} \left[\exp \left\{ -\frac{1}{2} [\theta'(dI - M)\theta + \beta'(eI - H)\beta - 2r'\theta - 2t'\beta] \right\} \right] \\
&\stackrel{(a)}{\geq} K_1 \mathbb{E}_{(\theta, \beta|r^0, t^0)} \left[\exp \left\{ -\frac{1}{2} \sum_{j=1}^p [d\theta_j^2 + e\beta_j^2 - 2r_j\theta_j - 2t_j\beta_j] \right\} \right] \\
&\stackrel{(b)}{=} K_1 \prod_{j=1}^p \mathbb{E}_{(\theta_j, \beta_j|r^0, t^0)} \left[\exp \left\{ -\frac{1}{2} [d\theta_j^2 + e\beta_j^2 - 2r_j\theta_j - 2t_j\beta_j] \right\} \right] \\
&= K_1 \prod_{j=1}^p \sum_{i \in \{-1, 0, 1\}} \mathbb{E} \left[\exp \left\{ -\frac{1}{2} [d\theta_j^2 + e\beta_j^2 - 2r_j\theta_j - 2t_j\beta_j] \right\} \middle| b_j = i, r^0, t^0 \right] \Pr(b_j = i|r^0, t^0) \\
&\geq K_1 \prod_{j=1}^p \min_{i \in \{-1, 0, 1\}} \underbrace{\mathbb{E} \left[\exp \left\{ -\frac{1}{2} [d\theta_j^2 + e\beta_j^2 - 2r_j\theta_j - 2t_j\beta_j] \right\} \middle| b_j = i, r^0, t^0 \right]}_{\mathcal{I}_{ij}}
\end{aligned}$$

where $K_1 = (2\pi)^{-2p} |dI - M|^{\frac{1}{2}} |eI - H|^{\frac{1}{2}} \exp\{-\frac{1}{2}[r'(dI - M)^{-1}r + t'(eI - H)^{-1}t]\}$. (a) follows from the fact that M and H are both semi-positive definite and (b) uses the conditional independence over $\{(\theta_j, \beta_j)\}_{j=1}^p$ given (r^0, t^0) .

When $i = 0$:

$$\begin{aligned}
\mathcal{I}_{0j} &= \mathbb{E}[\exp\{-\frac{1}{2}[e\beta_j^2 - 2t_j\beta_j]\} | b_j = 0, r^0, t^0] \\
&\geq \min \left\{ \exp\{-\frac{1}{2}[e\kappa_j^2 - 2t_j\kappa_j]\}, \exp\{-\frac{1}{2}[e\kappa_j^2 + 2t_j\kappa_j]\} \right\} := f_{0j}(r, t)
\end{aligned}$$

When $i = 1$:

$$\begin{aligned}
\mathcal{I}_{1j} &= \mathbb{E}[\exp\{-\frac{1}{2}[(d+e)\beta_j^2 - 2(r_j + t_j + d\kappa_j)\beta_j + d\kappa_j^2 + 2r_j\kappa_j]\} | b_j = 1, r^0, t^0] \\
&= \frac{\sqrt{\frac{d+e}{2\pi}}}{1 - \Phi[\sqrt{d+e}(\kappa_j - \mu_j^0)]}
\end{aligned}$$

$$\begin{aligned}
& \cdot \int_{\kappa_j}^{\infty} \exp \left\{ -\frac{1}{2} [2(d+e)\beta_j^2 - 2(r_j + t_j + d\kappa_j + (d+e)\mu_j^0)\beta_j \right. \\
& \quad \left. + d\kappa_j^2 + 2r_j\kappa_j + (d+e)(\mu_j^0)^2] \right\} d\beta_j \\
&= \frac{\sqrt{\frac{d+e}{2\pi}}}{1 - \Phi[\sqrt{d+e}(\kappa_j - \mu_j^0)]} \\
& \cdot \int_{\kappa_j}^{\infty} \exp \left\{ -\frac{2(d+e)}{2} \left(\beta_j - \frac{r_j + t_j + d\kappa_j + (d+e)\mu_j^0}{2(d+e)} \right)^2 \right\} d\beta_j \\
& \cdot \exp \left\{ \frac{(r_j + t_j + d\kappa_j + (d+e)\mu_j^0)^2}{4(d+e)} \right\} \exp \left\{ -\frac{d\kappa_j^2 + 2r_j\kappa_j + (d+e)(\mu_j^0)^2}{2} \right\} \\
&= \frac{1/\sqrt{2}}{1 - \Phi[\sqrt{d+e}(\kappa_j - \mu_j^0)]} \cdot \left[1 - \Phi \left(\frac{\kappa_j - \frac{r_j + t_j + d\kappa_j + (d+e)\mu_j^0}{2(d+e)}}{1/\sqrt{2(d+e)}} \right) \right] \\
& \cdot \exp \left\{ \frac{(r_j + t_j + d\kappa_j + (d+e)\mu_j^0)^2}{4(d+e)} \right\} \exp \left\{ -\frac{d\kappa_j^2 + 2r_j\kappa_j + (d+e)(\mu_j^0)^2}{2} \right\} \\
&\geq \frac{1}{\sqrt{2}} \Phi \left[\frac{\frac{r_j + t_j + d\kappa_j + (d+e)\mu_j^0}{2(d+e)} - \kappa_j}{1/\sqrt{2(d+e)}} \right] \exp \left\{ -\frac{d\kappa_j^2 + 2r_j\kappa_j + (d+e)(\mu_j^0)^2}{2} \right\} \\
&\stackrel{(a)}{\geq} \frac{1}{\sqrt{2}} \Phi \left[\frac{\frac{r_j + t_j + d\kappa_j}{2(d+e)} - \frac{1}{2}(\sqrt{\tilde{d}} + |\phi_j + \psi_j + d\kappa_j|) - \kappa_j}{1/\sqrt{2(d+e)}} \right] \\
& \cdot \exp \left\{ -\frac{d\kappa_j^2 + 2r_j\kappa_j + \frac{(\sqrt{\tilde{d}} + |\phi_j + \psi_j + d\kappa_j|)^2}{d+e}}{2} \right\} \\
&:= f_{1j}(r, t),
\end{aligned}$$

where (a) uses the fact that on $\mathcal{G}_{\tilde{d}}$, we have

$$|\mu_j^0| \leq \frac{|r_j^0 + t_j^0| + |\phi_j + \psi_j + d\kappa_j|}{d+e} \leq \frac{\sqrt{\tilde{d}} + |\phi_j + \psi_j + d\kappa_j|}{d+e}.$$

When $i = -1$: Similar to the $i = 1$ case, we can find a lower bound $f_{-1j}(r, t)$ for \mathcal{I}_{-1j} .

To sum up, we have proved that

$$\pi(r, t | r^0, t^0) \geq K_1 \prod_{j=1}^p \min_{i \in \{-1, 0, 1\}} f_{ij}(r, t), \quad \forall (r^0, t^0) \in \mathcal{G}_{\bar{d}},$$

which immediately leads to the minorization condition.

B Additional Results

B.1 Alternative Algorithm for Sampling Anti-correlation Gaussian

We now describe another efficient algorithm to sample from the anti-correlation Gaussian when $M = X'\Omega X$. Since $dI - X'\Omega X$ is positive definite, we have the following converging series:

$$(I - d^{-1}X'\Omega X)^{-1} = \sum_{k=0}^{\infty} (d^{-1}X'\Omega X)^k.$$

When truncating the right-hand side at K , we have:

$$\sum_{k=0}^K (d^{-1}X'\Omega X)^k = [I - (d^{-1}X'\Omega X)^{K+1}](I - d^{-1}X'\Omega X)^{-1}, \quad (\text{B.1})$$

where the relative error term $\|(d^{-1}X'\Omega X)^{K+1}\|_2 \leq \rho^K$, with $\rho = \lambda_p(X'\Omega X)/d$. Therefore, with a selected D and a numeric tolerance ϵ , we can control ρ and find out a suitable truncation $\hat{K} = \log_{\rho} \epsilon$. In our code, we use $\epsilon = 10^{-8}$, and $\rho = 2/3$ leading to $\hat{K} = 45$.

To generate a Gaussian with mean 0 and covariance as in (B.1), we can run the following algorithm, starting from a p -element $\gamma = 0$.

1. Simulate $\eta_1 \sim \mathcal{N}(0, I_p)$, $\eta_2 \sim \mathcal{N}(0, I_n)$,
2. Update $\gamma \leftarrow \eta_1 + d^{-1}X'\Omega^{1/2}\eta_2 + (d^{-1}X'\Omega X)\gamma$.

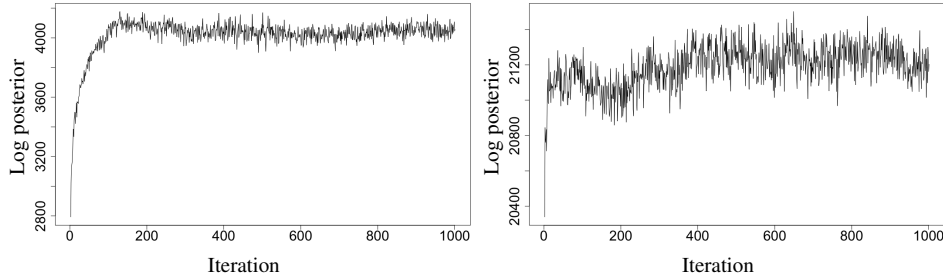
And it is not hard to see that each iteration increases K by 2, therefore, we only need to run the above algorithm for 23 iterations. Afterward, we set

$$r = (dI - X'\Omega X)d^{-1/2}\gamma + (dI - X'\Omega X)\theta,$$

which yields a Gaussian with mean $(dI - X'\Omega X)\theta$, variance numerically very close to $(dI - X'\Omega X)$.

B.2 Fast Convergence of the Anti-correlation Gaussian Blocked Sampler

We investigate the convergence speed of the anti-correlation Gaussian blocked sampler. We use the linear regression simulation setting with $n = 300$, $\rho = 0.5$, and $p \in \{1000, 5000\}$. Figure 5 shows the trace plots of log-posterior density during the burn-in stage. In both settings, the log-posterior density reaches stationarity within the first 500 iterations.

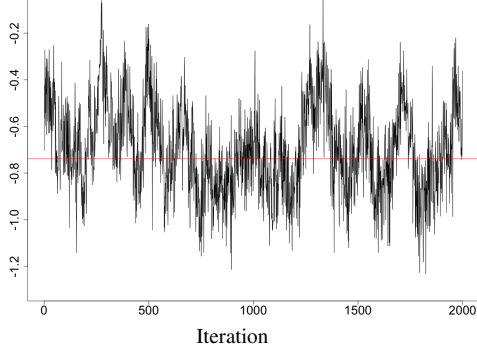


(a) Log posterior density for $p = 1000$. (b) Log posterior density for $p = 5000$.

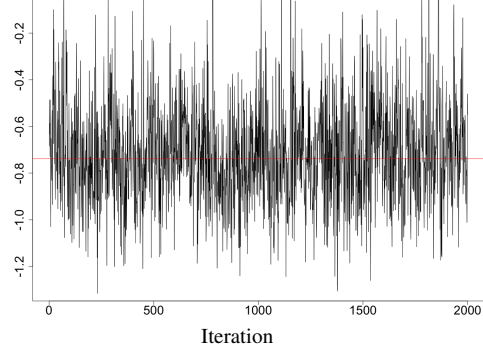
Figure 5: Trace plots of the log-posterior densities during the burn-in stage.

B.3 Additional Simulation for Estimating Soft-thresholded Gaussian Process

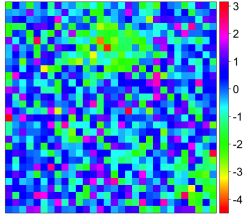
We conduct a simulation study for comparing the performance of the anti-correlation blocked Gibbs sampler and the Metropolis-Hastings within Gibbs algorithm (Kang et al. (2018), implemented in the R package ‘STGP’). We generate a 30 by 30 image from a soft-thresholded Gaussian process and then add Gaussian noise to each pixel. We run both algorithms for 3,000 iterations, and treat the first 1,000 as burn-ins. The results are shown in Figure 6. In terms of the mixing, the trace plots show that the Metropolis-Hastings within Gibbs algorithm has slightly faster mixing — although their implementation involves some C++ code, likely due to the high cost of Cholesky decomposition. Both methods yield similar image estimates that are smooth and sparse, with $\text{MSE}=0.02$ for the anti-correlation Gaussian and $\text{MSE}=0.04$ for the MH-within-Gibbs sampler.



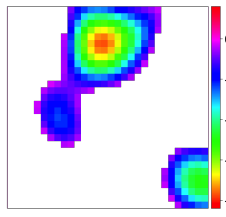
(a) Trace plot of θ_{116} for the anti-correlation Gaussian. The horizontal line denotes the ground truth.



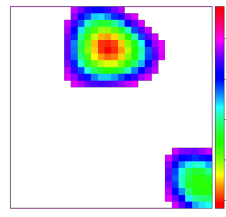
(b) Trace plot of θ_{116} for the MH within Gibbs sampler. The horizontal line denotes the ground truth.



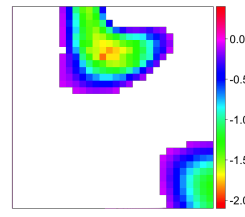
(c) Simulated data y .



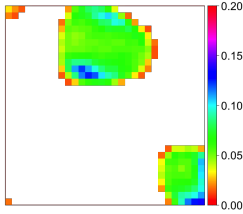
(d) Ground truth θ .



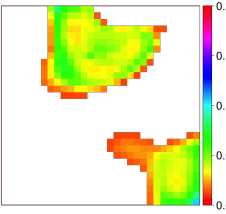
(e) Posterior estimate $\hat{\theta}$ produced by the anti-correlation Gaussian.



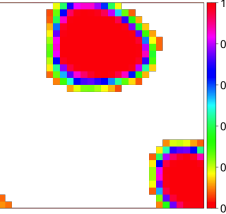
(f) Posterior estimate $\hat{\theta}$ produced by the MH-within-Gibbs sampler.



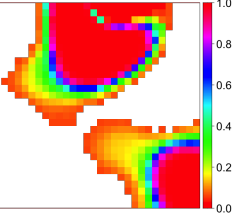
(g) Point-wise posterior variances for $\hat{\theta}$ produced by the anti-correlation Gaussian. MH-within-Gibbs sampler.



(h) Point-wise posterior variances for $\hat{\theta}$ produced by the MH-within-Gibbs sampler.



(i) $P(\theta_j \neq 0|y)$ produced by the anti-correlation Gaussian.



(j) $P(\theta_j \neq 0|y)$ produced by the MH-within-Gibbs sampler.

Figure 6: Trace plots, data, ground truth, posterior estimates, point-wise variances, and probabilities that an entry of θ is non-zero.

B.4 Benchmark: Sampling Truncated Multivariate Gaussian using Anti-correlation Gaussian

A comparison regarding the computational efficiency is conducted between the anti-correlation Gaussian and the `rtmvnorm()` function in the R package `tmvtnorm` (See [Wilhelm and Manjunath \(2010\)](#) for details). The argument “algorithm” in the function is set to be ‘gibbsR’ for a fair comparison in R language; otherwise, it uses Fortran to accelerate the function. We sample from p -dimensional truncated multivariate Gaussian distribution with zero mean, identity covariance matrix, and truncation area $R = \prod_{i=1}^p (-4, -3]$. For such specifications, rejection sampling breaks down even when p is as small as 10. We conducted 20 simulations with $p = 10$ for each algorithm. For each simulation, we do 12,000 iterations with 2,000 burn-ins and record the total clock wall time (in seconds). Figure 7 presents the trace plots of one randomly selected element of the parameter and compares the effective sample size per computing time (ESS/s) for anti-correlation Gaussian and `rtmvnorm`. Both algorithms enjoy fast mixing; however, anti-correlation Gaussian has an average ESS/s more than twice the average ESS/s for `rtmvnorm` across the 20 replications.

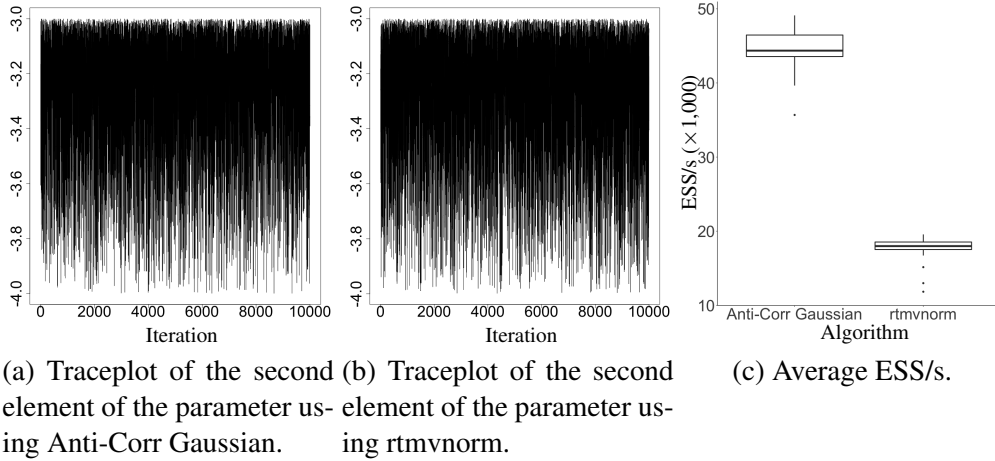


Figure 7: Traceplots and effective sample size per computing time (ESS/s) for anti-correlation Gaussian Gibbs sampler and `rtmvnorm`.

B.5 Stochastic Search Variable Selection (SSVS) Algorithm in Linear Regression

For the original spike-and-slab priors, the stochastic search variable selection algorithm (George and McCulloch, 1995) (a collapsed Gibbs sampler) enjoys excellent mixing and fast computing speed. On the other hand, the SSVS algorithm is limited to linear models that assume iid latent binary events $b_j = 1(\theta_j \neq 0)$ for $j = 1, \dots, p$, whereas our algorithm can be applied to general settings with dependent b_j 's. For example, in a soft-thresholded Gaussian process prior, there is a strong dependency between $\theta_s = 0$ and $\theta_{s'} = 0$ if the two spatial locations s and s' are close to each other. We provide a comparison between SSVS and anti-correlation Gaussian under the linear regression setting as in Section 5.1 with $p = 500$, $c = 3$, and $\rho = 0.5$. For SSVS, we use the 'lm.spike()' function in the R package 'BoomSpikeSlab' (Scott and Varian, 2014). Figure 8 shows that both anti-correlation Gaussian and SSVS work well in terms of the estimation accuracy of θ , while SSVS has a faster mixing.

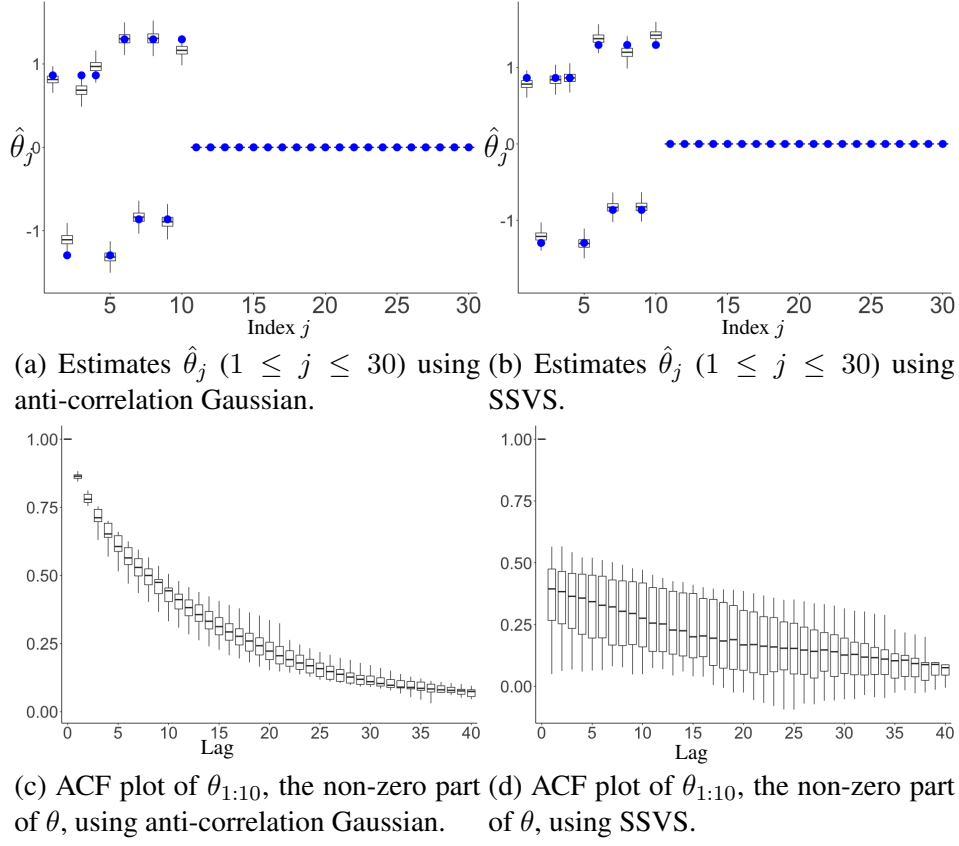


Figure 8: Estimates and ACF plots for anti-correlation Gaussian and SSVS. The blue points denote the ground truth. Each box on the plots of estimates incorporates all sample values after the burn-in stage.

B.6 Mixing under Different Values of Tuning Parameters d and e

We empirically assess the effects of the values of d (or e) on the mixing. We use the linear regression simulation setting with $p = 50$, $\rho = 0.5$, and $n = 300$ for experiments. Since $d\sigma^2$ should be larger than $\lambda_p(X^T X)$, we pick $d = \lambda_p(X^T X)/\sigma^2 + \varepsilon$. When ε takes value from $\{10^{-6}, 10^{-4}, 10^{-2}, 1, 10\}$, we see almost no difference in terms of mixing performance. When $\varepsilon = 100$, the algorithm fails to converge to the ground truth, likely due to numerical overflow.

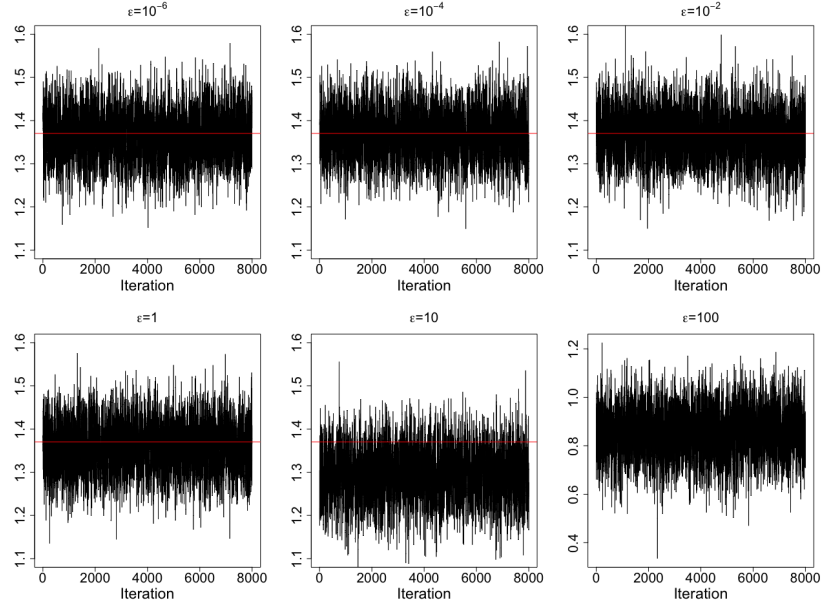


Figure 9: Under $d = \lambda_p(X^T X)/\sigma^2 + \varepsilon$ with $\varepsilon \in \{10^{-6}, 10^{-4}, 10^{-2}, 1, 10, 100\}$, the mixings of anti-correlation blocked Gibbs sampler have almost no difference.